IWSCFF 19-28

SPACECRAFT FORMATION AND ORBIT CONTROL USING ATTITUDE-DEPENDENT SOLAR RADIATION PRESSURE

Ethan R. Burnett*[*] and Hanspeter Schaub[†]

This paper introduces a model for spacecraft formation dynamics subject to attitude-dependent solar radiation pressure (SRP) disturbance, with the SRP model accounting for both absorption and specular/diffuse reflection. Spacecraft attitude is represented in Modified Rodriguez Parameters (MRPs), which have desirable properties over other attitude parameterizations. The model is derived and tested, then control examples are shown for hypothetical spacecraft with generally realistic optical parameters. This approach has applications to both formation control and to orbit maintenance. The results demonstrate the feasibility of SRP-based formation and rendezvous control in orbits around small bodies and in high orbits around the Earth such as the GEO belt.

INTRODUCTION

Solar radiation pressure (SRP) is the driving force for solar sails, but it is typically viewed as a disturbance force and not a control parameter for typical modern spacecraft. However, in environments where differential solar radiation pressure is sufficiently strong on the scale of the relative motion dynamics, small sustained variations in attitude can be used to harness this perturbation for control – even for spacecraft with realistic optical parameters. While not particularly suitable in low-Earth orbits, the efficacy of this control method becomes much greater for multi-spacecraft formations sufficiently far from the planet. In this region, the spacecraft are not subject to strong disturbances from higher-order gravitational effects or drag due to the rarefied atmosphere. SRP-based control also becomes a feasible option for formations in orbit around small bodies such as asteroids, comets, and moons.

The possibility of using small attitude changes for formation-keeping is appealing because of the potential for saved thruster fuel. It is also valuable because the differential SRP force between identical spacecraft can achieve the incredibly small values necessary for real-time and high-precision formation-keeping around small asteroids and comets. Even the smallest commercially available ion thrusters are often too powerful for continuous use in station-keeping in these environments, requiring them to be used in a pulsed control strategy almost like chemical thrusters. This contradicts the nature of their design for very long-duration burns, reducing efficiency and accelerating wear. Other design solutions are available to partially mitigate this issue, such as pulsed plasma thrusters (PPTs), but these are nowhere near as efficient as other forms of electric propulsion. In this context,

[*]PhD student, Ann and H.J. Smead Department of Aerospace Engineering Sciences, University of Colorado Boulder, CO, 80309

[†]Professor, Glenn Murphy Endowed Chair, Ann and H.J. Smead Department of Aerospace Engineering Sciences, University of Colorado Boulder, CO, 80309

SRP-based control would be preferred over any type of electric propulsion, and can be implemented on spacecraft with traditional geometry and surface materials.

The topic of natural SRP-perturbed orbital dynamics has been frequently studied, especially in the vicinity of small bodies.[1] Many works use a cannonball SRP model, and focus on finding stable orbits while assuming the force variation with attitude is not significant.[2,3] Some works also discuss orbit-attitude coupling in the uncontrolled dynamics, or the coupled effects of multiple perturbations.[4–6] Recent work by Kenshiro Oguri and Jay McMahon focuses on SRP-based orbit control around asteroids.[7] The optical force SRP model used in their work is essentially equivalent to the one used here, but their approach is otherwise quite different. Their work studies orbit control via a chosen subset of the orbit elements, namely semimajor axis and inclination. The optimal attitude for control is parameterized by two angles, whose values are obtained numerically based on the current system state. The paper makes multiple novel analytical arguments that provide intuition about the controlled orbital dynamics – including attitude constraints to prevent orbital escape, and even an analytic upper bound for the time of flight for landing on an asteroid using SRP-based control.

It is worth noting that SRP-based control has also been extensively studied for solar sails, but this work usually makes restrictive assumptions about the spacecraft optical properties. While interesting work has been done to study the natural and controlled orbital dynamics using the SRP force, this paper is focused on the topic of orbital formation control, for which spacecraft with unremarkable geometry can still produce sufficient differences in SRP force to use it as a relative position and velocity control parameter.

A desirable approach for formation control would be to use a model that requires only occasional updates of the formation state differences and the spacecraft orbital elements of one or more of the spacecraft. These state differences could be provided directly from measurements in local-vertical local-horizontal (LVLH) components. The option to perform most control computations in advance would also be desirable. Ideally, a model accounting for the evolution of the perturbed orbit and the linearized SRP-perturbed differential dynamics will naturally enable sufficiently reliable situational awareness even with low navigation update frequency. Lastly, a linearized approach leverages the smallness of the formation geometry on the scale of the spacecraft orbits. It is also amenable to a linearly optimal LQR control approach – in which the optimal gain schedule can be computed in advance of the maneuver, or in a receding-horizon manner.

The notion of using SRP for spacecraft control is not new. Several highly successful missions have used the attitude variations in SRP force to enhance the capability of a spacecraft otherwise not explicitly designed to harness the disturbance. The K2 mission was able to make use of SRP effects to extend the life of the Kepler space telescope mission, which was suffering from attitude control under-actuation due to reaction wheel failure. This was done by achieving and maintaining an orientation to passively minimize the SRP disturbance along the roll axis.[8] The Messenger mission to Mercury used SRP for precision orbit control, which is particularly notable and relevant to this work. In that mission, pre-planned attitude and solar array articulations were used to improve the accuracy of Mercury flybys.[9] This was done in an open-loop fashion, but closed-loop control would be desirable. Closed-loop control should be readily achievable using SRP models with varying levels of fidelity.

This paper focuses on developing an accurate linearized time-varying (LTV) model of formation dynamics subject to attitude-dependent SRP forces. The model uses the chief-deputy notation commonly used in spacecraft formation flying, in which the motion of one spacecraft (the deputy) is described with respect to another (the chief), in a local chief-centered frame. The model may be updated with chief orbit elements with any desired frequency. The analytical approach in this paper naturally allows for the evolution of the spacecraft orbit elements to be approximated for relatively long timespans. This model can easily be combined with components of other models to account for additional system perturbations.[10] While it is assumed that updated relative heading, range, and range-rate data is periodically available for the spacecraft in the formation, the relative position and velocity can be efficiently integrated between measurements using the linearized model. By incorporating accurate and computationally efficient approximation of system evolution into the model, significant decoupling of the tasks of control and navigation is achievable. Overall, the developments in this paper are a step towards enabling a highly flexible, simple formation control strategy suitable for closed-loop SRP-based spacecraft formation control.

After the linearized model is developed, a linearly optimal control strategy is designed for small attitude departures from a reference orientation. For simplicity in developing the proof-of-concept simulations, the model is implemented with a single facet only, but the approach can be easily generalized to a multi-facet spacecraft model. The model developed in this paper could be adapted and extended to find use in future multi-spacecraft missions to asteroids and comets, and will also be useful for formation control or orbit maintenance in high-altitude orbits about the Earth, such as the GEO belt.

SPACECRAFT FORMATION DYNAMICS WITH SOLAR RADIATION PRESSURE

The force due to solar radiation pressure on a body surface element A_i is given below:[11]

$$\boldsymbol{F}_{S_i} = -P(R)H_i(\hat{\boldsymbol{u}})A_i\left[\left(\rho_i s_i\left(2\hat{\boldsymbol{n}}\hat{\boldsymbol{n}} - \overline{\overline{\boldsymbol{I}}}\right) + \overline{\overline{\boldsymbol{I}}}\right)\cdot\hat{\boldsymbol{u}}\left(\hat{\boldsymbol{u}}\cdot\hat{\boldsymbol{n}}_i\right) + a_{2i}\hat{\boldsymbol{n}}_i\left(\hat{\boldsymbol{n}}_i\cdot\hat{\boldsymbol{u}}\right)\right] \tag{1}$$

with

$$P(R) \approx \frac{G_1}{R^2} \tag{2}$$

$$a_{2i} = B(1-s_i)\rho_i + (1-\rho_i)B \tag{3}$$

The function $P(R)$ is the solar radiation pressure at distance R, and G_1 is the solar radiation force constant at 1 AU. The specular and diffuse reflectivity coefficients are s_i and ρ_i, and B is the Lambertian scattering coefficient, $\hat{\boldsymbol{u}}$ is the unit vector to the sun, and $H(\hat{\boldsymbol{u}})$ is a visibility delta function, equal to 1 or 0, depending on whether or not the face is directly illuminated by sunlight.

For simplicity and generality, this analysis neglects the effects of secondary reflections from other surfaces. However, a realistic treatment of the body optical properties (B, s_i, ρ_i) is important.

The SRP force can be modeled by considering the sum of the forces on all illuminated facets. The results in this paper use a single-facet model of a spacecraft. However, it is emphasized that this method can be directly generalized to a spacecraft with fixed geometry and multiple illuminated facets. Summing over the contributions of all body area elements, an approximate model of the net SRP force vector on the spacecraft is obtained:

$$\boldsymbol{F}_S = -P(R)A\left(\left(\overline{a}_2\cos\beta + 2\overline{\rho s}\cos^2\beta\right)\hat{\boldsymbol{n}} + (1-\overline{\rho s})\cos\beta\hat{\boldsymbol{u}}\right) \tag{4}$$

where $\cos\beta = \hat{\boldsymbol{u}}\cdot\hat{\boldsymbol{n}}$, A is a projected area term, and $\hat{\boldsymbol{n}}$ is the corresponding equivalent normal unit vector. The terms $\overline{a}_2$, $\overline{\rho}$, and $\overline{s}$ are illuminated body-averaged optical parameters. This replaces the multi-facet SRP force model with a single-plate SRP force model at some reference orientation. It is always possible to obtain an equivalent single-plate model representation of the resultant SRP force acting on a spacecraft, for which the sum of the $\hat{\boldsymbol{n}}_i$ components of the resultant SRP force acts along $\hat{\boldsymbol{n}}$, and the total $\hat{\boldsymbol{u}}$ component is also reproduced. However, the extent to which attitude-dependent SRP force variations of the single plate correctly model the true spacecraft SRP force variations is situation dependent. Accuracy would be highly dependent on spacecraft geometry and the optical properties of the surface facets.

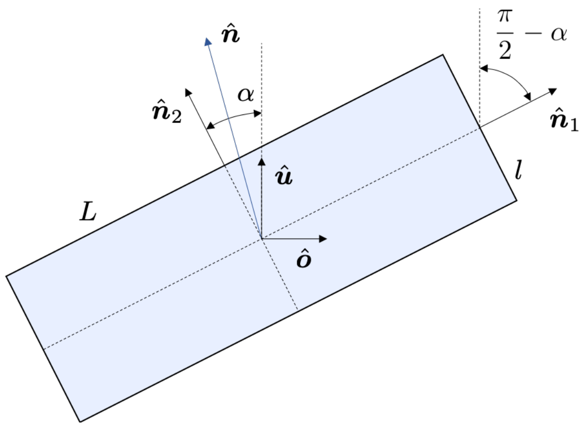

Figure 1. Simple Spacecraft Representation

While the single-plate representation used in this paper will be extended for multi-facet spacecraft models in future work, a short analysis demonstrates that the assumptions in this paper are reasonable for a proof-of-concept. Figure 1 is a simplified representation of averaging over the illuminated spacecraft area to create a single-plate approximation. This figure is used to provide perspective on the accuracy of such a procedure by examining the error in the resultant normal vector $\hat{\boldsymbol{n}}$ of the single-plate approximation.

The spacecraft body is a rectangular prism of dimensions $l \times L \times W$. The unit vector $\hat{\boldsymbol{u}}$ points toward the sun, and the unit vector $\hat{\boldsymbol{o}}$ is orthogonal to $\hat{\boldsymbol{u}}$. For analytical simplicity body is oriented such that only two faces are illuminated, so $\hat{\boldsymbol{n}}_i \cdot \hat{\boldsymbol{u}} > 0$ only for $i = 1, 2$. If the optical properties of the two illuminated facets are similar, the single-plate model will have a resultant normal vector $\hat{\boldsymbol{n}}$ given below:

$$\hat{\boldsymbol{n}} = \frac{\sum_i \hat{\boldsymbol{n}}_i A_i \left(\hat{\boldsymbol{n}}_i \cdot \hat{\boldsymbol{u}}\right)}{\left\|\sum_i \hat{\boldsymbol{n}}_i A_i \left(\hat{\boldsymbol{n}}_i \cdot \hat{\boldsymbol{u}}\right)\right\|} = \frac{\hat{\boldsymbol{n}}_1 l \sin\alpha + \hat{\boldsymbol{n}}_2 L \cos\alpha}{\sqrt{L^2 \cos^2\alpha + l^2 \sin^2\alpha}}$$
$$= \frac{1}{\sqrt{L^2 \mathrm{c}^2\alpha + l^2 \mathrm{s}^2\alpha}} \begin{pmatrix} (l - L)\sin\alpha\cos\alpha \\ L\cos^2\alpha + l\sin^2\alpha \end{pmatrix} \tag{5}$$

where the final expression is resolved into components $n_{(1)}$ and $n_{(2)}$ along $\hat{\boldsymbol{o}}$ and $\hat{\boldsymbol{u}}$, respectively. For a counterclockwise rotation through a small additional angle δ, the resultant normal vector $\hat{\boldsymbol{n}}'$ will still be given by Eq. (5), but with rotation angle $\alpha' = \alpha + \delta$ and unit vectors $\hat{\boldsymbol{n}}_1'$ and $\hat{\boldsymbol{n}}_2'$ appropriately rotated counterclockwise by δ from their reference orientation depicted in Figure 1. On the other hand, the rotation by δ of the normal vector of the single plate representation is given below:

$$\hat{\boldsymbol{n}}' \approx \begin{pmatrix} n_{(1)}\cos\delta - n_{(2)}\sin\delta \\ n_{(1)}\sin\delta + n_{(2)}\cos\delta \end{pmatrix} \tag{6}$$

The difference between this approximate result and the actual result provides a simplified single measure how well the single-plate representation works. The accuracy is a function of reference offset angle α and the area of the two illuminated rectangular facets LW and lW. Note that there is no W dependency appearing for this example due to the orientation. For small angles δ, the error in the normal vector can be shown to be:

$$\boldsymbol{e}_{\hat{\boldsymbol{n}}} \approx \frac{1}{\left(L^2\mathrm{c}^2\alpha + l^2\mathrm{s}^2\alpha\right)^{3/2}} \begin{pmatrix} -\frac{1}{2}L\left(L + l + (L - l)\cos 2\alpha\right) \\ L(L-l)\sin\alpha\cos\alpha \end{pmatrix} l\delta \tag{7}$$

For a sun-facing reference orientation $\alpha \ll 1$, this yields the intuitive result of non-negligible error only in the $\hat{\boldsymbol{o}}$ direction:

$$\boldsymbol{e}_{\hat{\boldsymbol{n}}} \approx -\frac{l}{L}\delta\hat{\boldsymbol{o}} \tag{8}$$

This is an important result. As expected, the error in Eq. (7) also approaches zero as $l/L \to 0$. The single-plate representation becomes more accurate as the body becomes more plate-like, but it also can retain reasonable accuracy for $l/L \neq 0$ for near sun-facing reference orientations with $\alpha \ll 1$. For example, in the case of the small-angle restrictions of Eq. (8), for a 6U CubeSat with $l/L = 1/3$, the error is $\boldsymbol{e}_{\hat{\boldsymbol{n}}} \approx 0.0058\hat{\boldsymbol{o}}$ per degree of δ.

Similar analysis with the projected area and optical parameters can be carried out. This analysis could also be done in 3D with three facets, but the results are needlessly complex for this discussion. Future work will extend the methods in this paper to develop a control model that explicitly accounts for the SRP force on spacecraft with multiple illuminated facets, so no further discussion of single-plate approximations is needed.

Other approaches of modeling SRP acceleration variation for small angles are possible, such as a local linearization of the spherical harmonic series representation.[12] The purpose of this work is to demonstrate the feasibility of using attitude-dependent SRP acceleration for formation and rendezvous control, so studies of the control implications of SRP model fidelity are left for future work.

Problem Geometry and Coordinate Frames

Before continuing with the derivation of the linearized dynamics and control model, the primary coordinate frames must be defined. First, the primary body Hill frame H_P is defined by orthonormal vectors $\left\{\hat{\boldsymbol{u}}, \hat{\boldsymbol{H}} \times \hat{\boldsymbol{u}}, \hat{\boldsymbol{H}}\right\}$, where $\hat{\boldsymbol{u}}$ points from the planet toward the sun and $\hat{\boldsymbol{H}} = \boldsymbol{h}_p/h_p$ is defined by the planet's orbit angular momentum vector $\boldsymbol{h}_p$, normal to its orbit plane.

One can describe the rotation from the primary-centered Hill frame to the primary-centered inertial (N) frame through two angles:

$$[NH_P] = [R_1(\kappa)]\,[R_3(\varphi+\pi)]^\top = \begin{bmatrix} -\cos\varphi & \sin\varphi & 0 \\ -\sin\varphi\cos\kappa & -\cos\varphi\cos\kappa & \sin\kappa \\ \sin\varphi\sin\kappa & \cos\varphi\sin\kappa & \cos\kappa \end{bmatrix} \tag{9}$$

where κ is the obliquity of the ecliptic plane and φ is the argument of latitude, or the rotation angle (in the orbit plane) from the Vernal Equinox to the radial vector from the sun to the planet. For Earth, $\kappa \approx 23.5°$, and the N frame would be the typical Earth-centered inertial (ECI) frame.

Since this paper is focused on using SRP force for rendezvous and formation control, the controlled relative motion of two or more spacecraft is considered. The spacecraft labeling deputy and chief is commonly used in formation flying literature. The motions of one or more deputies relative to the chief are used to describe formation or rendezvous geometry without explicitly considering all individual spacecraft orbits. Note that one may arbitrarily decide which spacecraft is designated as the chief and which is the deputy. In this paper, the chosen representation for the relative state is to resolve the relative position

$$\Delta \boldsymbol{r} = [x, y, z]^\top \tag{10}$$

and velocity

$$\Delta \boldsymbol{r}' = [\dot{x}, \dot{y}, \dot{z}]^\top \tag{11}$$

in the chief-centered rotating local-vertical, local-horizontal (LVLH) frame. Here, $(\ )'$ denotes the derivative of a state quantity as seen in the LVLH frame. This frame rotates with the spacecraft orbit and is defined by orthonormal radial, along-track, and orbit-normal vectors $\{\hat{\boldsymbol{e}}_r, \hat{\boldsymbol{e}}_t, \hat{\boldsymbol{e}}_n\}$. The radial and normal unit vectors are defined in the usual way, in terms of the chief spacecraft position $\boldsymbol{r}$ and velocity $\boldsymbol{v}$: $\hat{\boldsymbol{e}}_r = \boldsymbol{r}/r$ and $\hat{\boldsymbol{e}}_n = \boldsymbol{r} \times \boldsymbol{v}/\|\boldsymbol{r} \times \boldsymbol{v}\|$.

Now a final rotation from the inertial frame to an orbiting spacecraft-centered local-vertical local-horizontal (LVLH frame) may be defined. The rotation $[H_S N]$ is given below in terms of the chief spacecraft orbit radial and angular momentum vectors $\boldsymbol{r}$ and $\boldsymbol{h}$, and equivalently in a 3–1–3 sequence in terms of the spacecraft orbit elements Ω, i, and θ:[13]

$$[H_S N] = \begin{bmatrix} \hat{\boldsymbol{r}}^\top \\ \frac{1}{rh}\left(r^2 \boldsymbol{v} - (\boldsymbol{v} \cdot \boldsymbol{r})\, \boldsymbol{r}\right)^\top \\ \hat{\boldsymbol{h}}^\top \end{bmatrix} \tag{12}$$

$$[H_S N] = \begin{bmatrix} \cos\Omega\cos\theta - \sin\Omega\sin\theta\cos i & \sin\Omega\cos\theta + \cos\Omega\sin\theta\cos i & \sin\theta\sin i \\ -\cos\Omega\sin\theta - \sin\Omega\cos\theta\cos i & -\sin\Omega\sin\theta + \cos\Omega\cos\theta\cos i & \cos\theta\sin i \\ \sin\Omega\sin i & -\cos\Omega\sin i & \cos i \end{bmatrix} \tag{13}$$

Thus, the rotation from H_P to H_S is:

$$[H_S H_P] = [H_S N]\,[N H_P] \tag{14}$$

With the system geometry and coordinate descriptions now defined, a control matrix $[B]$ can now be obtained, which maps deputy spacecraft attitude to accelerations in the LVLH frame. The uncontrolled dynamics of an SRP-perturbed multi-spacecraft formation are also considered to obtain the system matrix $[A]$. This complex derivation follows the control matrix derivation.

Linearized Attitude-based SRP Control

Modified Rodrigues Parameters (MRPs) are used to describe the spacecraft attitude, or the attitude of a single-plate model in this paper. These are a newer attitude description that are expressed in terms of the principal rotation elements (angle α and axis $\hat{\boldsymbol{e}}$):[13]

$$\boldsymbol{\sigma} = \tan\frac{\alpha}{4}\hat{\boldsymbol{e}} \tag{15}$$

The MRP attitude representation has the benefit of linearizing as $\boldsymbol{\sigma} \approx (\alpha/4)\,\hat{\boldsymbol{e}}$, providing a larger usable range for linear control than an angular representation.

The mapping to and from a general rotation matrix $[C]$ is given below:

$$[C] = [I_{3\times3}] + \frac{8[\tilde{\boldsymbol{\sigma}}]^2 - 4(1-\sigma^2)[\tilde{\boldsymbol{\sigma}}]}{(1+\sigma^2)^2} \tag{16}$$

$$\boldsymbol{\sigma} = \begin{pmatrix} \sigma_1 \\ \sigma_2 \\ \sigma_3 \end{pmatrix} = \frac{1}{\zeta\,(\zeta+2)} \begin{pmatrix} C_{23} - C_{32} \\ C_{31} - C_{13} \\ C_{12} - C_{21} \end{pmatrix} \tag{17}$$

where $\zeta = \sqrt{C_{11} + C_{22} + C_{33} - 1}$, $\sigma^{2n} = \left(\boldsymbol{\sigma}^\top \boldsymbol{\sigma}\right)^n$, and $[\tilde{\boldsymbol{\sigma}}]$ is the MRP skew-symmetric matrix.

To use the MRP formulation, the rotation of a vector in H_P components into the spacecraft body frame (B_S) components is defined in terms of two successive rotations. The first is a rotation $[C_1(\boldsymbol{\sigma}_r)]$ to the "reference" attitude, and the second is a rotation $[C_2(\boldsymbol{\sigma}_c)]$ to the current orientation, which is a controlled deviation from this reference attitude:

$$^{B_S}\boldsymbol{r} = [C_2(\boldsymbol{\sigma}_c)][C_1(\boldsymbol{\sigma}_r)]^{H_P}\boldsymbol{r} \tag{18}$$

The attitude deviation $\boldsymbol{\sigma}_c$ is the control parameter for attitude-based position control using SRP. This work assumes that the spacecraft attitude control system is fully capable of enforcing the needed attitude behavior.

From equation 4, substituting $\hat{\boldsymbol{n}} \cdot \hat{\boldsymbol{u}}$ for all $\cos\alpha$ terms, the force due to SRP is rewritten below in its H_P components using $^{H_P}\hat{\boldsymbol{n}} = [C_1(\boldsymbol{\sigma}_r)]^\top [C_2(\boldsymbol{\sigma}_c)]^{\top\, B_S}\hat{\boldsymbol{n}}$ and defining $^{B_S}\hat{\boldsymbol{n}} = \hat{\boldsymbol{e}}_1$ and $^{H_P}\hat{\boldsymbol{u}} = \hat{\boldsymbol{e}}_1$, where $\hat{\boldsymbol{e}}_1 = [1, 0, 0]^\top$:

$$\boldsymbol{F}_S = -P(R)A\left(\left(\overline{a}_2\,(\hat{\boldsymbol{n}} \cdot \hat{\boldsymbol{u}}) + 2\overline{\rho s}\,(\hat{\boldsymbol{n}} \cdot \hat{\boldsymbol{u}})^2\right)[C_1(\boldsymbol{\sigma}_r)]^\top [C_2(\boldsymbol{\sigma}_c)]^\top + (1 - \overline{\rho s})\,(\hat{\boldsymbol{n}} \cdot \hat{\boldsymbol{u}})\,[I_{3\times3}]\right)\hat{\boldsymbol{e}}_1 \tag{19}$$

To obtain the $[B]$ matrix, this equation must be linearized with respect to the control term $\boldsymbol{u} = \boldsymbol{\sigma}_c$. First, all control-associated parts are replaced with their expansions up to $\mathcal{O}(\sigma_c)$:

$$[C_2(\boldsymbol{\sigma}_c)] \approx [I_{3\times3}] - 4[\tilde{\boldsymbol{\sigma}}_c] \tag{20}$$

$$\hat{\boldsymbol{n}} \cdot \hat{\boldsymbol{u}} = \hat{\boldsymbol{e}}_1^\top [C_2(\boldsymbol{\sigma}_c)][C_1(\boldsymbol{\sigma}_r)]\hat{\boldsymbol{e}}_1 \approx \hat{\boldsymbol{e}}_1^\top \left([C_1(\boldsymbol{\sigma}_r)] - 4[\tilde{\boldsymbol{\sigma}}_c][C_1(\boldsymbol{\sigma}_r)]\hat{\boldsymbol{e}}_1\right) \tag{21}$$

$$(\hat{\boldsymbol{n}} \cdot \hat{\boldsymbol{u}})^2 \approx \left(\hat{\boldsymbol{e}}_1^\top [C_1(\boldsymbol{\sigma}_r)]^\top \hat{\boldsymbol{e}}_1\right)\hat{\boldsymbol{e}}_1^\top \left([C_1(\boldsymbol{\sigma}_r)] - 8[\tilde{\boldsymbol{\sigma}}_c][C_1(\boldsymbol{\sigma}_r)]\hat{\boldsymbol{e}}_1\right) \tag{22}$$

Substituting Eqs. (20) – (22) into Eq. (19), expanding, and retaining only terms up to $\mathcal{O}(\sigma_c)$, the linearization of $\boldsymbol{F}_S$ is obtained:

$$\begin{aligned} \boldsymbol{F}_S \approx &- P(R)A\Big\{ \left(\overline{a}_2 + 2\overline{\rho s}\hat{\boldsymbol{e}}_1^\top [C_1(\boldsymbol{\sigma}_r)]\hat{\boldsymbol{e}}_1\right)\left(\hat{\boldsymbol{e}}_1^\top [C_1(\boldsymbol{\sigma}_r)]\hat{\boldsymbol{e}}_1 \left([C_1(\boldsymbol{\sigma}_r)]^\top \left([I_{3\times3} + 4[\tilde{\boldsymbol{\sigma}}_c]\right)\right)\right) \\ &- 4\left(\overline{a}_2 + 4\overline{\rho s}\hat{\boldsymbol{e}}_1^\top [C_1(\boldsymbol{\sigma}_r)]\hat{\boldsymbol{e}}_1\right)\hat{\boldsymbol{e}}_1^\top [\tilde{\boldsymbol{\sigma}}_c][C_1(\boldsymbol{\sigma}_r)]\hat{\boldsymbol{e}}_1 [C_1(\boldsymbol{\sigma}_r)]^\top \\ &+ (1 - \overline{\rho s})\,\hat{\boldsymbol{e}}_1^\top \left([I_{3\times3}] - 4[\tilde{\boldsymbol{\sigma}}_c]\right)\hat{\boldsymbol{e}}_1 [I_{3\times3}]\Big\}\hat{\boldsymbol{e}}_1 \end{aligned} \tag{23}$$

This equation is linear in $\boldsymbol{\sigma}_c$, and is rearranged below so that the control vector $\boldsymbol{\sigma}_c$ is explicitly isolated:

$$\begin{aligned}\boldsymbol{F}_S = &- P(R)A\Big\{ \left(\overline{a}_2 + 2\overline{\rho s}C_{1(1,1)}\right)\left(C_{1(1,1)}[C_1(\boldsymbol{\sigma}_r)]^\top\right)\hat{\boldsymbol{e}}_1 \\ &- 4\left(\overline{a}_2 + 2\overline{\rho s}C_{1(1,1)}\right)\left(C_{1(1,1)}[C_1(\boldsymbol{\sigma}_r)]^\top[\tilde{\boldsymbol{e}}_1]\right)\boldsymbol{\sigma}_c \\ &- 4\left(\overline{a}_2 + 4\overline{\rho s}C_{1(1,1)}\right)\left([C_1(\boldsymbol{\sigma}_r)]^\top[\hat{\boldsymbol{e}}_1\hat{\boldsymbol{e}}_1^\top][C_1(\boldsymbol{\sigma}_r)]^\top[\tilde{\boldsymbol{e}}_1]\right)\boldsymbol{\sigma}_c \\ &+ (1-\overline{\rho s})\hat{\boldsymbol{e}}_1 + 4(1-\overline{\rho s})[\hat{\boldsymbol{e}}_1\hat{\boldsymbol{e}}_1^\top][\tilde{\boldsymbol{e}}_1]\boldsymbol{\sigma}_c\Big\}\end{aligned} \tag{24}$$

where the shorthand notation $C_{1(1,1)} = \hat{\boldsymbol{e}}_1^\top[C_1(\boldsymbol{\sigma}_r)]\hat{\boldsymbol{e}}_1$ is used. If the reference orientation is sun-facing, then $[C_1(\boldsymbol{\sigma}_r)] = [I_{3\times3}]$ and a simpler form is obtained:

$$\boldsymbol{F}_S = -P(R)A\left\{(1+\overline{\rho s}+\overline{a}_2)\hat{\boldsymbol{e}}_1 - 4(\overline{a}_2+2\overline{\rho s})[\tilde{\boldsymbol{e}}_1]\boldsymbol{\sigma}_c\right\} \tag{25}$$

From this result, the $[B]$ matrix can be isolated for the system resolved in H_P:

$$[B] = 4\frac{P(R)A}{m}\begin{bmatrix} & \boldsymbol{0}_{4\times3} & \\ 0 & 0 & -\overline{a}_2 - 2\overline{\rho s} \\ 0 & \overline{a}_2 + 2\overline{\rho s} & 0\end{bmatrix} \tag{26}$$

The $[B]$ matrix for a more general reference orientation can be readily obtained by isolating the control-associated terms in Eq. (24). This can also be easily resolved in any desired frame by using the appropriate rotation matrices. Note that in the case of linearization about a sun-facing reference, the $[B]$ matrix for the system resolved in H_P predicts zero acceleration will be produced along the $\hat{\boldsymbol{u}}$ direction due to small controlled attitude variations. In reality, a small acceleration will be produced, but this is not captured by the linearization. This suggests that motion along the $\hat{\boldsymbol{u}}$ direction is instantaneously uncontrollable with linear control. However, investigations later in the paper show that the system is still fully controllable.

Linearized Relative Motion Dynamics under SRP

The SRP-perturbed uncontrolled relative orbital motion behavior of the spacecraft is now derived. Because the SRP-based control is enabled by deviations from a reference attitude that is assumed to be fixed in the H_P frame, this analysis assumes that the SRP-based differential acceleration between the deputy and chief spacecraft is negligible. This implicitly assumes that the deputy and chief geometry and optical characteristics are similar. In this case, with both spacecraft at the same reference orientation, the only manifestation of the SRP acceleration is on the kinematics of the chief LVLH frame. Note that depending on the dynamic environment, this effect may be overshadowed by other disturbance accelerations.

The angular velocity of the perturbed LVLH frame may be described in terms of the perturbed orbit element rates:[14]

$$\boldsymbol{\omega}_H = \frac{\mathrm{d}\Omega}{\mathrm{d}t}\hat{\boldsymbol{K}} + \frac{\mathrm{d}i}{\mathrm{d}t}\frac{\hat{\boldsymbol{K}}\times\hat{\boldsymbol{e}}_n}{\|\hat{\boldsymbol{K}}\times\hat{\boldsymbol{e}}_n\|} + \frac{\mathrm{d}\theta}{\mathrm{d}t}\hat{\boldsymbol{e}}_n \tag{27}$$

The orbit element rates are obtained using the variational equations in their Gaussian form to yield the osculating rates due to the SRP perturbation, resolved in local radial, along-track, and cross-track components:

$$\boldsymbol{a}_{\text{SRP}} = R_{\text{SRP}}\hat{\boldsymbol{e}}_r + T_{\text{SRP}}\hat{\boldsymbol{e}}_t + N_{\text{SRP}}\hat{\boldsymbol{e}}_n \tag{28}$$

$$\frac{\mathrm{d}\Omega}{\mathrm{d}t} = \frac{r\sin\theta}{h\sin i} N_{\text{SRP}} \tag{29a}$$

$$\frac{\mathrm{d}i}{\mathrm{d}t} = \frac{rcos\theta}{h} N_{\text{SRP}} \tag{29b}$$

$$\frac{\mathrm{d}\theta}{\mathrm{d}t} = \frac{\mathrm{d}\omega}{\mathrm{d}t} + \frac{\mathrm{d}f}{\mathrm{d}t} = \frac{h}{r^2} - \frac{r\sin\theta\cos i}{h\sin i} N_{\text{SRP}} \tag{29c}$$

The argument of latitude is used to avoid the possibility of small denominators in the variational equations for near-circular orbits. The argument of latitude rate has two components: the "unperturbed" argument of latitude rate $\dot{\theta}_u = h/r^2$, and a component due to the regression of the node from which θ is measured.[15] The expression for N_{SRP} may be obtained using the rotation from H_P to H_S, and the SRP disturbance force resolved in H_P components:

$$N_{\text{SRP}} = \frac{1}{m}\hat{\boldsymbol{e}}_3^\top [H_S N] [N H_P] \boldsymbol{F}_S \tag{30}$$

$$N_{\text{SRP}} = -P(R)\frac{A}{m}\left(\frac{(1-\overline{\rho s})}{C_{1(1,1)}} + \overline{a}_2 + 2\overline{\rho s}C_{1(1,1)}\right)C_{1(1,1)}\left(\hat{\boldsymbol{e}}_3^\top [H_S N] [N H_P] [C_1(\boldsymbol{\sigma}_r)]^\top \hat{\boldsymbol{e}}_1\right) \tag{31}$$

$$N_{\text{SRP}} = -P(R)\frac{A}{m}\left(\frac{(1-\overline{\rho s})}{C_{1(1,1)}} + \overline{a}_2 + 2\overline{\rho s}C_{1(1,1)}\right)C_{1(1,1)}\left(\hat{\boldsymbol{e}}_\xi^\top [C_1(\boldsymbol{\sigma}_r)]^\top \hat{\boldsymbol{e}}_1\right) \tag{32}$$

where the unit vector $\hat{\boldsymbol{e}}_\xi$ is not a function of θ due to the problem geometry:

$$\hat{\boldsymbol{e}}_\xi = \begin{pmatrix} \sin\kappa\sin\varphi\cos i - \sin\Omega\cos\varphi\sin i + \cos\Omega\cos\kappa\sin\varphi\sin i \\ \sin\kappa\cos\varphi\cos i + \sin\Omega\sin\varphi\sin i + \cos\Omega\cos\kappa\cos\varphi\sin i \\ \cos\kappa\cos i - \cos\Omega\sin\kappa\sin i \end{pmatrix} \tag{33}$$

Assuming the primary body orbit radius R is nearly constant and that the reference orientation is stationary as seen in the H_P frame, the only time-varying term in Eq. (32) is the primary body's argument of latitude, φ. Generally, this time scale will be much slower than the spacecraft orbit period about the primary body.

By applying the transport theorem twice with angular velocity given by Eq. (27), the kinematics of the perturbed LVLH frame are given in radial, along-track, and cross-track components:

$$\begin{aligned} \Delta\ddot{\boldsymbol{r}} = &\left(\ddot{x} - \dot{\omega}_n y - 2\omega_n\dot{y} - \omega_n^2 x + \omega_n\omega_r z\right)\hat{\boldsymbol{e}}_r \\ &+ \left(\ddot{y} + \dot{\omega}_n x + 2\omega_n\dot{x} - \left(\omega_n^2 + \omega_r^2\right) y - \dot{\omega}_r z - 2\omega_r\dot{z}\right)\hat{\boldsymbol{e}}_t \\ &+ \left(\ddot{z} + \omega_n\omega_r x + \dot{\omega}_r y + 2\omega_r\dot{y} - \omega_r^2 z\right)\hat{\boldsymbol{e}}_n \end{aligned} \tag{34}$$

where the angular velocity has also been resolved into its LVLH components:

$$\omega_r = \dot{\Omega}\frac{\sin i}{\sin\theta} \tag{35a}$$

$$\omega_t = 0 \tag{35b}$$

$$\omega_n = \dot{\theta}_u = h/r^2 \tag{35c}$$

The term $\Delta\ddot{\boldsymbol{r}}$ represents the differential perturbing accelerations. If only the SRP differential acceleration is considered, then, in the case of the earlier listed assumptions, this term is due only to the differential gravity, which is assumed to be a two-body potential for now:

$$\Delta\ddot{\boldsymbol{r}}_{J_0} = \frac{\mu}{r^3}\begin{pmatrix} 2x \\ -y \\ -z \end{pmatrix} \tag{36}$$

The choice of local Cartesian/curvilinear coordinates for treatment of the perturbed relative motion problem has led to one important limitation: large chief orbit eccentricities introduce significant analytical difficulties to the derivation, for multiple reasons. While such problems are still analytically tractable, this derivation is restricted to cases of $e \approx 0$ (near-circular orbits) and $\dot{a} \approx 0$ (negligible changes to orbit specific energy). This dynamical model can theoretically be adapted for perturbed eccentric orbits, assuming $\dot{e} \approx 0$ still holds, and that all ρ terms are updated to account for the variations in the chief radius. Note that writing $\dot{e} \approx 0$ only implies the assumption that the effects from $\dot{e}$ are small compared to the first-order effects of the solar radiation pressure. However, this will not always be the case. Both the long and short-term effects of solar radiation pressure on eccentricity are discussed extensively in other sources.[1] Relaxing of the aforementioned assumptions and further potential developments of the model are left to future work.

To first order in the SRP terms, assuming $\dot{a} \approx 0$ and $\dot{e} \approx 0$, it can be shown that the only nonzero angular acceleration term is $\dot{\omega}_r$, given below with the nonzero angular velocity squared terms:

$$\dot{\omega}_r = n\frac{\sin i}{\sin\theta}\left(\frac{\mathrm{d}}{\mathrm{d}\theta}\left(\dot{\Omega}\right) - \dot{\Omega}\frac{\cos\theta}{\sin\theta}\right) + \dot{\varphi}\frac{\sin i}{\sin\theta}\frac{\mathrm{d}}{\mathrm{d}\varphi}\left(\dot{\Omega}\right) \tag{37}$$

$$\omega_n\omega_r = n\rho^{-3/2}\dot{\Omega}\frac{\sin i}{\sin\theta} \tag{38}$$

$$\omega_n^2 = \frac{h^2}{r^4} \tag{39}$$

where $\rho = r/a$ and n is the orbital mean motion. From the near-circular orbit assumption and the assumption $\dot{a} \approx 0$, it is implied that $r(t) \approx a$, thus $\dot{\theta}_p \approx n$ and $\rho \approx 1$. These assumptions will not be valid for long time spans if the SRP disturbance acceleration is large enough to significantly change the chief orbit. Evaluating Eqs. (37) – (39), all nonzero kinematic terms are presented below, explicitly in terms of N_{SRP}:

$$\omega_r = \frac{r}{h}N_{\text{SRP}},\ \omega_n = \frac{h}{r^2} \tag{40}$$

$$\dot{\omega}_r = \dot{\varphi}\frac{r}{h}\frac{\mathrm{d}}{\mathrm{d}\varphi}\left(N_{\text{SRP}}\right) \tag{41}$$

$$\omega_n\omega_r = n\rho^{-3/2}\frac{r}{h}N_{\text{SRP}},\ \omega_n^2 = \frac{h^2}{r^4} \tag{42}$$

The final linearized relative motion equations are obtained and presented below in matrix-vector form, resolved in the chief-centered LVLH frame, H_S.

$$\begin{pmatrix} \ddot{x} \\ \ddot{y} \\ \ddot{z} \end{pmatrix} = \begin{bmatrix} h^2/r^4 + 2\frac{\mu}{r^3} & 0 & -n\rho^{-3/2}\frac{r}{h}N_{\text{SRP}} \\ 0 & h^2/r^4 - \frac{\mu}{r^3} & \dot{\varphi}\frac{r}{h}\frac{\mathrm{d}}{\mathrm{d}\varphi}\left(N_{\text{SRP}}\right) \\ -n\rho^{-3/2}\frac{r}{h}N_{\text{SRP}} & -\dot{\varphi}\frac{r}{h}\frac{\mathrm{d}}{\mathrm{d}\varphi}\left(N_{\text{SRP}}\right) & -\frac{\mu}{r^3} \end{bmatrix}\begin{pmatrix} x \\ y \\ z \end{pmatrix} + \begin{bmatrix} 0 & 2\frac{h}{r^2} & 0 \\ -2\frac{h}{r^2} & 0 & 2\frac{r}{h}N_{\text{SRP}} \\ 0 & -2\frac{r}{h}N_{\text{SRP}} & 0 \end{bmatrix}\begin{pmatrix} \dot{x} \\ \dot{y} \\ \dot{z} \end{pmatrix} \tag{43}$$

If small variations in the chief orbit radius are known, and any resulting terms are of the same order as linear SRP-associated terms, then the substitution of these variations may be desirable. Otherwise, if $r \approx a \, \forall t$, and e is small, the expression may be simplified further:

$$\begin{pmatrix} \ddot{x} \\ \ddot{y} \\ \ddot{z} \end{pmatrix} = \begin{bmatrix} 3n^2 & 0 & -n\frac{a}{h}N_{\text{SRP}} \\ 0 & 0 & \dot{\varphi}\frac{a}{h}\frac{\mathrm{d}}{\mathrm{d}\varphi}\left(N_{\text{SRP}}\right) \\ -n\frac{a}{h}N_{\text{SRP}} & -\dot{\varphi}\frac{a}{h}\frac{\mathrm{d}}{\mathrm{d}\varphi}\left(N_{\text{SRP}}\right) & -n^2 \end{bmatrix} \begin{pmatrix} x \\ y \\ z \end{pmatrix} + \begin{bmatrix} 0 & 2n & 0 \\ -2n & 0 & 2\frac{a}{h}N_{\text{SRP}} \\ 0 & -2\frac{a}{h}N_{\text{SRP}} & 0 \end{bmatrix} \begin{pmatrix} \dot{x} \\ \dot{y} \\ \dot{z} \end{pmatrix} \tag{44}$$

The position and velocity-associated matrices in Eq. (44) are denoted as $[A_p]$ and $[A_v]$, respectively. Reusing the state representation $\boldsymbol{x} = [x, y, z, \dot{x}, \dot{y}, \dot{z}]^\top$, for which one may write $\dot{\boldsymbol{x}} = [A(t)]\boldsymbol{x}$, the time-varying $[A]$ matrix is:

$$[A] = \begin{bmatrix} 0_{3\times3} & I_{3\times3} \\ A_p & A_v \end{bmatrix} \tag{45}$$

with all components of the linear model defined, the linearized relative orbital motion dynamics can now be expressed in their usual form:

$$\dot{\boldsymbol{x}} = [A(t)]\boldsymbol{x} + [B(t)]\boldsymbol{u} \tag{46}$$

The $[A]$ matrix terms are given in Eqs. (44) – (45). The control-associated $[B]$ matrix is given in Eq. (26), with the lower 3×3 sub-matrix now pre-multiplied by $[H_S H_P]$ to resolve the resultant control accelerations in the LVLH frame components.

APPLICATION TO SPACECRAFT FORMATION CONTROL

This section discusses and demonstrates the implementation of the new SRP-perturbed relative orbital motion model for control.

Linear SRP-Based Formation and Rendezvous Control

Control in this paper is performed using the Linear Quadratic Regulator (LQR), which is for the design of a control input $\boldsymbol{u}$ that minimizes the finite-time cost function shown below, under the action of the linearized dynamics $\dot{\boldsymbol{x}} = [A]\boldsymbol{x} + [B]\boldsymbol{u}$.[16]

$$J = \frac{1}{2}\int_{t_0}^{t_f} \left(\boldsymbol{x}^\top[Q]\boldsymbol{x} + \boldsymbol{u}^\top[R]\boldsymbol{u}\right) \mathrm{d}t + \frac{1}{2}\boldsymbol{x}_f^\top[S_f]\boldsymbol{x}_f \tag{47}$$

The solution is given below:

$$\boldsymbol{u} = -[K_x]\boldsymbol{x} \tag{48}$$

The time-varying gain matrix $[K_x]$ is given in terms of $[S]$, obtained by solving the Riccati differential equation with final condition $[S(t_f)] = [S_f]$:

$$[K_x] = [R]^{-1}[B]^\top[S] \tag{49}$$

$$[\dot{S}] + [S][A] + [A]^\top[S] - [S][B][R]^{-1}[B]^\top[S] + [Q] = [0] \tag{50}$$

Controllability Analysis

Before the SRP-based control is simulated, controllability analysis provides some insight into the problem. For completeness, the time-varying effects of the SRP perturbation are included in the $[A]$ matrix for the relative motion dynamics.

For an LTV system with n states, if the following is satisfied, the system is controllable:[16]

$$\text{rank}\left([B_0(t), B_1(t), \ldots, B_{n-1}(t)]\right) = n \tag{51}$$

where $[B_0] = [B]$ and all other elements are given by the following:

$$[B_{i+1}(t)] = [A(t)][B_i(t)] - \frac{\mathrm{d}}{\mathrm{d}t}[B_i(t)] \tag{52}$$

The rank of the controllability matrix, if less than n, determines the dimension of the controllable subspace.

To facilitate this discussion for SRP-based control, the $[B]$ matrix is now resolved into H_S:

$$[B] = \begin{bmatrix} 0_{3\times 3} \\ [H_S N][N H_P][B_C] \end{bmatrix} \tag{53}$$

where $[B_C]$ is the constant part of the $[B]$ matrix:

$$\begin{aligned}[B_C] = 4P(R)\frac{A}{m}\Big(&\left(\overline{a}_2 + 2\overline{\rho s}C_{1(1,1)}\right) C_{1(1,1)}[C_1(\boldsymbol{\sigma}_r)]^\top[\tilde{\boldsymbol{e}}_1] - (1-\overline{\rho s})[\hat{\boldsymbol{e}}_1\hat{\boldsymbol{e}}_1^\top][\tilde{\boldsymbol{e}}_1] \\ &+ \left(\overline{a}_2 + 4\overline{\rho s}C_{1(1,1)}\right)[C_1(\boldsymbol{\sigma}_r)]^\top[\hat{\boldsymbol{e}}_1\hat{\boldsymbol{e}}_1^\top][C_1(\boldsymbol{\sigma}_r)]^\top[\tilde{\boldsymbol{e}}_1]\Big)\end{aligned} \tag{54}$$

If the reference orientation is sun-facing, then $[C_1(\boldsymbol{\sigma}_r)] = [I_{3\times 3}]$ and a much simpler form is obtained for $[B_C]$:

$$[B_C] = 4P(R)\frac{A}{m}\left(\overline{a}_2 + 2\overline{\rho s}\right)[\tilde{\boldsymbol{e}}_1] \tag{55}$$

For this controllability analysis, it is assumed that the reference orientation is sun-facing. The rotation from H_P to H_S is time-varying, and thus the $[B]$ matrix will be time-varying as well. Furthermore, the $[A]$ matrix is time-varying. The time-varying terms in the $[A]$ matrix obtained from Eq. (44) can be expected to evolve slowly compared to the time scale of the relative orbital motion dynamics.

Using the SRP-perturbed system $[A]$ matrix, the controllability matrix is obtained in terms of the $[B_i(t)]$ sub-matrices:

$$[B_i(t)] = [B_i'(t)][B_C] = \begin{bmatrix} [B'_{i(u)}(t)] \\ [B'_{i(l)}(t)] \end{bmatrix}[B_C] \tag{56}$$

where the time-varying portion $[B_i'(t)]$ can be shown to obey the following recursive relationship and initial values:

$$[B'_{i+1}(t)] = \begin{bmatrix} [B'_{i(l)}(t)] - \frac{d}{dt}\left([B'_{i(u)}(t)]\right) \\ [A_p][B'_{i(u)}(t)] + [A_v][B'_{i(l)}(t)] - \frac{d}{dt}\left([B'_{i(l)}(t)]\right) \end{bmatrix} \tag{57}$$

$$[B'_{0(u)}(t)] = [0_{3\times3}],\ [B'_{0(l)}(t)] = [H_S H_P] \tag{58}$$

Using Eq. (57), and recalling $[B_0(t)] = [B(t)]$, the next two sub-matrices are shown analytically:

$$[B_1(t)] = \begin{bmatrix} [H_S H_P] \\ [A_v][H_S H_P] - [H_S H_P][\tilde{\omega}_{S,P}] \end{bmatrix} [B_C] \tag{59}$$

$$[B_2(t)] = \begin{bmatrix} [A_v][H_S H_P] - 2[H_S H_P][\tilde{\omega}_{S,P}] \\ [A_p][H_S H_P] + [A_v]^2[H_S H_P] - 2[A_v][H_S H_P][\tilde{\omega}_{S,P}] + [H_S H_P][\tilde{\omega}_{S,P}]^2 - [\dot{A}_v][H_S H_P] \end{bmatrix} [B_C] \tag{60}$$

where $[\tilde{\omega}_{S,P}]$ is an angular velocity term associated with the rotating frames:

$$\frac{\mathrm{d}}{\mathrm{d}t}\left([H_S H_P]\right) = [H_S H_P][\tilde{\omega}_{S,P}] \tag{61}$$

The matrix $[\tilde{\omega}_{S,P}]$ is skew-symmetric, with the components of the angular velocity of frame H_P relative to H_S, expressed in H_P components. Note that it is assumed that angular acceleration terms are zero because the effect of rotating frame angular acceleration terms is quite small for near-circular planetary and spacecraft orbits. Thus, $[\dot{\tilde{\omega}}_{S,P}] \approx [0_{3\times3}]$.

The symbolic expressions for each sub-matrix were obtained via MATLAB and saved as functions. To enforce the zero angular acceleration condition, the time-varying angular terms were truncated to their linear approximations, $\theta \approx \theta_0 + nt$ and $\varphi \approx \varphi_0 + \dot{\varphi}t$. The final expression for the controllability matrix is far too long and complex to include here.

Table 1 gives hypothetical parameters for evaluating the controllability matrix, and for the first set of simulation results to follow this controllability analysis. The optical parameters for this first result are values corresponding to a completely reflective surface,[17] but adding absorption doesn't affect the conclusion of the controllability analysis. This hypothetical simulation data is representative of some high-altitude orbit over a large asteroid. Only two-body gravity and SRP perturbations are implemented in the truth model, since this paper is primarily concerned with the solar radiation pressure perturbation, which would be a dominant disturbance at this altitude.

Table 1. Simulation 1 Physical Parameters

Parameter	Value
$\boldsymbol{\text{œ}}_0 = (a, e, i, \Omega, \theta)$	$200, 0.0, 86.0°, 0.0°, 0.0°$
$\delta\boldsymbol{\text{œ}}_0 = (\delta a, \delta e, \delta i, \delta\Omega, \delta\theta)$	$0.0, 0.00125, 0.05°, 0.0°, 0.0°$
Optical constants	$\frac{A}{m} = 0.5\text{m}^2/\text{kg}, \overline{B} = 0.8, \overline{s} = 0.7, \overline{\rho} = 0.3$
Primary Body Orbit Radius	$R = 3.5904 \times 10^8$km (2.4AU)
Primary Body Orbit Angles	$\kappa = 4°, \varphi_0 = 90°$
Primary Body Physical Parameters	$d = 40$km, $\rho = 2.119\text{g/cm}^3, m = 7.1 \times 10^{16}$kg

Using the parameters in Table 1, the rank of the controllability matrix may be obtained for various times in the simulation. Numerical results show that the rank of the controllability matrix is consistently 6, using the default tolerance in MATLAB. Lowering the tolerance (e.g. to 1×10^{-10}), the rank of the controllability matrix reduces to 4. These numerical results suggest that the system is fully controllable, with kinematic coupling enabling weak controllability of the spacecraft motion along $\hat{\boldsymbol{u}}$.

Testing the SRP-Perturbed Relative Motion Model

First, results are presented to demonstrate that the dynamical model obtained in this paper works as expected. Namely, the model given in Eq. (44) was simulated for the data given in Table 1, along with a nonlinear truth model. The results are given in Figure 2. Note that there is close agreement between the SRP model and the nonlinear truth model for the 6 orbits simulated. This shows that the linearized SRP model is properly accounting for the SRP disturbance acceleration's effects.

Controlled Simulation Results

With the efficacy of the linearized dynamical model demonstrated, finite-time LQR control is now implemented to obtain the optimal control signals $\boldsymbol{u}(t) = \boldsymbol{\sigma}_c(t)$. Of particular interest is the full controllability of the system implied by the analysis in the preceding section. It was hypothesized that controllability is weakest in the projection of the motion along $\hat{\boldsymbol{u}}$. Setting the relative motion to take place near the terminator plane allows the motion along $\hat{\boldsymbol{u}}$ to be easily investigated. Without treating the out-of-plane associated elements of the $[Q]$ matrix differently from the in-plane associated elements, simulation results show that the motion in the z direction fails to settle. However, by over-weighing the cost of z and $\dot{z}$ in the dynamics, the controller takes a strategy that seeks to minimize the motion in this mode, by delaying the settling of the x and y motion.

The first simulation demonstrates relative motion regulation control to a chief in a terminator orbit. The non-optical physical constants and initial conditions are unchanged from the uncontrolled simulation - thus are given in Table 1. The control parameters and the new optical parameters for this simulation are given in Table 2.

Table 2. Control Parameters and Optical Parameters for Simulation 1

Parameter	Value
Q	$Q = I_{6\times6},$ except $Q(3,3) = Q(6,6) = 60$
R	$100I_{3\times3}$
S_f	$I_{6\times6}$
$t_0, \Delta t, t_f$	$t_0 = 0, \Delta t = 10, t_f = 2581510$ (29.88 days)
Optical constants	$\frac{A}{m} = 0.5\text{m}^2/\text{kg}, \overline{B} = 0.6, \overline{s} = 0.25, \overline{\rho} = 0.3$

The position deviations and control signals are given in Figures 4 and 5. The results show that for this case, the controller functions as intended – successfully controlling the deputy spacecraft to very near the origin of the LVLH frame, over the course of one month. This is done with $< 10^\circ$ attitude deviations from the sun-pointing direction. This is important in the context of this work, because the attitude variations must remain small in order for the single-plate SRP model to be accurate.

The second simulation demonstrates control to change a GEO orbit longitude by 0.544°, or 20 km in the along-track direction, over the course of 30 days. The optical parameters are the same as in the first simulation, but the other physical parameters and the new control parameters are different. These are given in Tables 3 and 4 respectively. This simulation neglects the perturbative effects of lunar and solar gravity, which manifest via a long term (53 year) precession and nutation of the orbit.[18] In this particular case, a scale analysis of the lunar gravity perturbation will show that there would be sufficient control authority to cancel such perturbations in addition to controlling the spacecraft to the desired location.

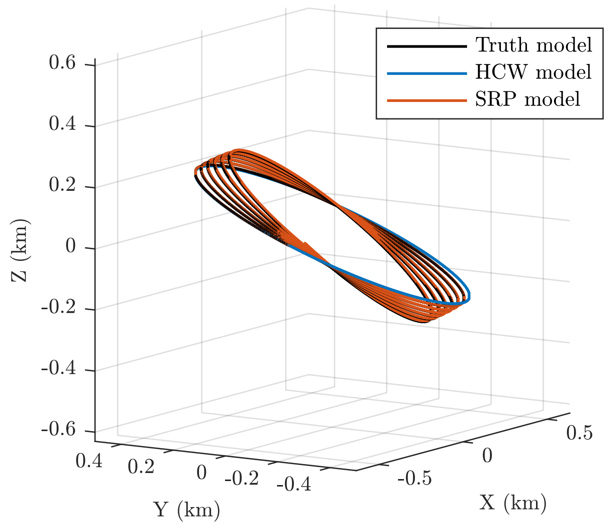

Figure 2. SRP-Perturbed Relative Motion

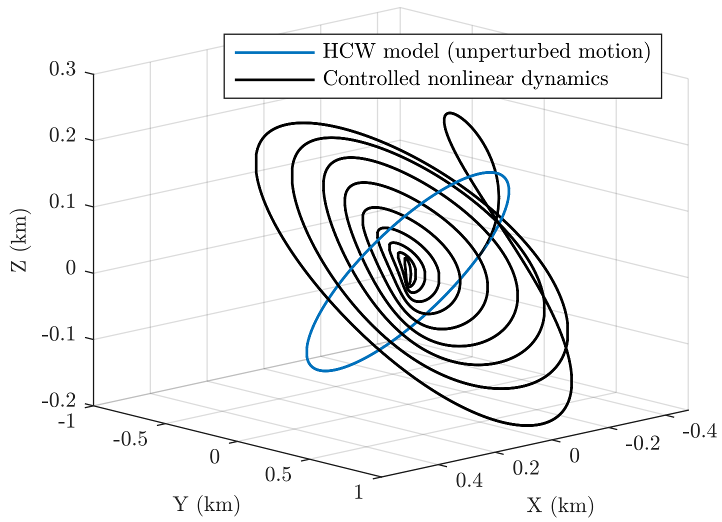

Figure 3. SRP-Based Control of Relative Motion, Case 1

The motion in LVLH x and y components is given in Figure 6. The z motion is quite insignificant in this case, so it is not shown. Note that the scale of the x motion is magnified in the figure to show the bowed nature of the trajectory followed, and to clearly show the oscillations in the radial direction. Also note the overshoot in the y direction followed by the slow settling behavior around the origin. There are two time scales of the settling behavior. Much of the separation is settled in the along-track direction within 15 orbits, but the control action in the remaining orbits slowly dampens out the oscillations mainly in the x and y components. The large final cost on the relative state ensures that in the final 3-4 orbits, the relative motion is further settled.

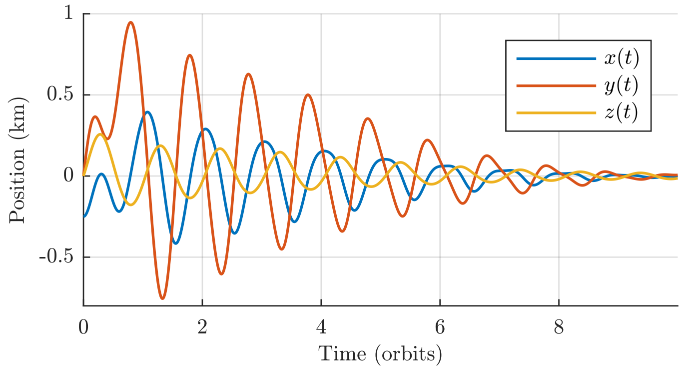

Figure 4. Controlled Position, Case 1

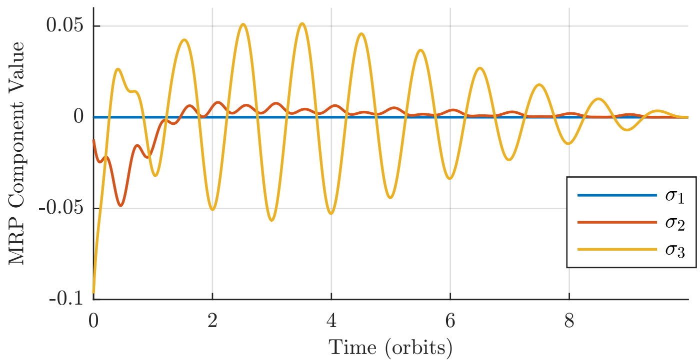

Figure 5. Control Signals, Case 1

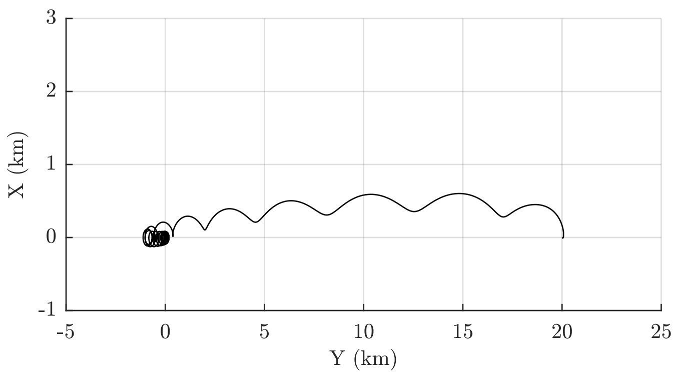

Figure 6. SRP-Based Control of Relative Motion, Case 2

These results suggest that relatively large maneuvers in the GEO belt are possible with SRP-based linear control, assuming sufficient time is available for such maneuvers. Faster settling results would likely be possible through iteration on the current selection of control parameters, but these results are an adequate demonstration of capability. The results from cases 1 and 2 show that both closed-loop rendezvous control and larger changes to a GEO orbit using a virtual chief are

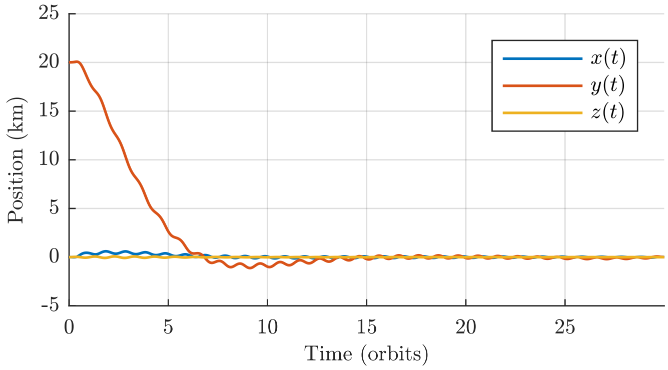

Figure 7. Controlled Position, Case 2

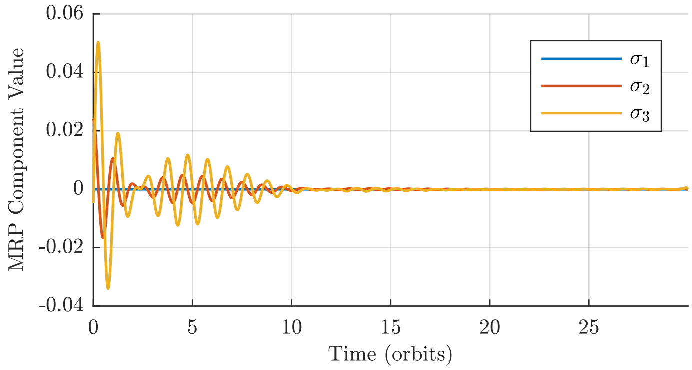

Figure 8. Control Signals, Case 2

Table 3. Simulation 2 Physical Parameters

Parameter	Value
$\text{œ}_0 = (a, e, i, \Omega, \theta)$	$42157, 0.0, 0.0°, 0.0°, 0.0°$
$\delta\text{œ}_0 = (\delta a, \delta e, \delta i, \delta\Omega, \delta\theta)$	$0.0, 0.0, 0.0°, 0.0°, 0.544°$
Primary Body Orbit Radius	$R = 1.496 \times 10^8$km (1.0AU)
Primary Body Orbit Angles	$\kappa = 23.5°, \varphi_0 = 90°$
Primary Body Physical Parameters	$r = 6371$ km, $\mu = 398600$ km$^3/s^2$

Table 4. Control Parameters and Optical Parameters for Simulation 2

Parameter	Value
Q	$0.5 I_{6\times 6}$
R	$10^5 I_{3\times 3}$
S_f	$S_f = 10^8 I_{6\times 6}$, except $S_f(1,1) = 10^{10}$ & $S_f(4,4) = 10^{11}$
$t_0, \Delta t, t_f$	$t_0 = 0, \Delta t = 80, t_f = 2584240$ (30 days)
Optical constants	$\frac{A}{m} = 0.5$m^2/kg, $\overline{B} = 0.6, \overline{s} = 0.25, \overline{\rho} = 0.3$

possible using small sustained attitude variations to change the resultant SRP disturbance force. This is simulated for spacecraft with relatively realistic area-to-mass ratios and unremarkable (neither highly reflective or absorptive) optical properties. Simulations with smaller area-to-mass ratios still display the same characteristic behavior, but with longer time spans needed to achieve the same control objectives.

CONCLUSIONS

This paper derives a new relative motion model accounting for the effects of the solar radiation pressure (SRP) disturbance acceleration on spacecraft relative motion. The kinematics of the SRP-perturbed chief orbit are absorbed into the linearized system $[A(t)]$ matrix to accommodate infrequent updates of the chief orbit parameters. The model demonstrates the feasibility of SRP-based control in multiple environments of interest for spacecraft with unremarkable geometry and surface optical properties. The model is derived from an existing multi-facet model of SRP force, obtaining an illuminated body averaged single-plate model that should be valid for small angular attitude deviations, especially for spacecraft with large solar arrays, or otherwise relatively flat spacecraft. Numerical simulations of SRP-based control for spacecraft with unremarkable geometric and optical properties establish the feasibility of the use of attitude-dependent SRP force for formation and rendezvous control.

Future work will explore refinements to the methods used in this work, and will detail the limitations of the model and control strategy used in this work. An in-depth study how performance changes with differing optical properties would also be useful. Future work will also include higher-fidelity multi-facet spacecraft SRP modeling that is valid for larger attitude variations, and explorations of how to account for independent articulation of solar arrays in a box-wing spacecraft model. Finally, the study of uncontrolled SRP-perturbed formation dynamics may also continue, with updated models to ease the restrictions made by assumptions in deriving this model.

A multi-fidelity modeling approach could enable a low-level control strategy (linear or otherwise) to be corrected for high precision SRP-based control. Look-up tables generated in advance (or series fits of such data) could take place of the linearized approximation of the attitude-dependent variations in the magnitude and direction of the resultant SRP acceleration. This work is thus the first step towards a goal of accurate high-fidelity SRP-based formation and orbit control.

ACKNOWLEDGEMENTS

This work was supported by the U.S. Department of Defense through the National Defense Science and Engineering Graduate Fellowship (NDSEG) Program.

REFERENCES

[1] D. J. Scheeres, *Orbital Motion in Strongly Perturbed Environments*. Springer-Verlag Berlin Heidelberg, 2012.

[2] H. Dankowicz, "Some Special Orbits in the Two-Body Problem with Radiation Pressure," *Celestial Mechanics and Dynamical Astronomy*, Vol. 58, No. 4, 1994, pp. 353–370.

[3] S. M. Byram and D. J. Scheeres, "Stability of Sun-Synchronous Orbits in the Vicinity of a Comet," *Journal of Guidance, Control, and Dynamics*, Vol. 32, No. 5, 2009, pp. 1550–1559.

[4] S. Kikuchi, K. C. Howell, Y. Tsuda, and J. Kawaguchi, "Orbit-attitude coupled motion around small bodies: Sun-synchronous orbits with Sun-tracking attitude motion," *Acta Astronautica*, Vol. 140, 2017, pp. 34–48.

[5] G. Misra, M. Izadi, A. Sanyal, and D. J. Scheeres, "Coupled Orbit-Attitude Dynamics and Relative State Estimation of Spacecraft Near Small Solar System Bodies," *Advances in Space Research*, Vol. 57, No. 8, 2016, pp. 1747–1761.

[6] D. Lantukh, R. P. Russell, and S. B. Broschart, "Heliotropic Orbits at Oblate Asteroids: Balancing Solar Pressure and J2 Perturbations," *Celestial Mechanics and Dynamical Astronomy*, Vol. 121, No. 171-190, 2015.

[7] K. Oguri and J. W. McMahon, "SRP-based Orbit Control with Application to Small Body Landing," *AAS/AIAA Astrodynamics Specialist Conference*, 2018.
[8] H. e. al., "The K2 Mission: Characterization and Early Results," *Publications of the Astronomical Society of the Pacific*, 2014.
[9] D. J. O'Shaughnessy, J. V. McAdams, K. E. Williams, and B. R. Page, "Fire Sail: Messenger's use of Solar Radiation Pressure for Accurate Mercury Flybys," *AAS Spaceflight Mechanics Meeting*, American Astronautical Society, 2009.
[10] E. R. Burnett and E. A. Butcher, "Linearized Relative Orbital Motion Dynamics in a Rotating Second Degree and Order Gravity Field," *AAS/AIAA Astrodynamics Specialist Conference*, American Astronautical Society, 2018.
[11] D. J. Scheeres, "The dynamical evolution of uniformly rotating asteroids subject to YORP," *Icarus*, Vol. 188, 2007, pp. 430–450.
[12] A. Farrés, D. Folta, and C. Webster, "Using Spherical Harmonics to Model Solar Radiation Pressure Accelerations," *AAS/AIAA Astrodynamics Specialist Conference*, American Astronautical Society, 2017.
[13] H. Schaub and J. L. Junkins, *Analytical Mechanics of Space Systems*. Reston, VA: AIAA Education Series, 4th ed., 2018.
[14] S. Casotto, "The Equations of Relative Motion in the Orbital Reference Frame," *Celestial Mechanics and Dynamical Astronomy*, Vol. 124, No. 3, 2016, pp. 215–234.
[15] J. E. Prussing and B. A. Conway, *Orbital Mechanics*. Oxford University Press, 2013.
[16] E. Sontag, *Mathematical Control Theory: Deterministic Finite Dimensional Systems*. Springer, 1998.
[17] C. R. McInnes, *Solar Sailing: Technology, Dynamics, and Mission Applications*. Springer-Verlag, 1999.
[18] P. Anderson, D. S. McKnight, F. D. Pentino, and H. Schaub, "Operational Considerations of GEO Debris Synchronization Dynamics," *66th International Astronautical Conference*, International Astronautical Federation, 2015.